Phonon dynamics in AV_2O_5 (A = Na,Ca,Mg,Cs) oxides

Z. V. Popović,[1,*] M. J. Konstantinović,[1] R. Gajić,[2] V. N. Popov,[3] M. Isobe,[4] Y. Ueda,[4] and V. V. Moshchalkov[1]

[1]*Laboratorium voor Vaste-Stoffysica en Magnetisme, Katholieke Universiteit Leuven, Celestijnenlaan 200D, B-3001 Leuven, Belgium*

[2]*Institute of Physics, 11080 Belgrade, P.O. Box 68, Yugoslavia*

[3]*Faculty of Physics, University of Sofia, 1126 Sofia, Bulgaria*

[4]*Institute for Solid State Physics, The University of Tokyo, 5-11-5 Kashiwanoha, Kashiwa, Chiba 277-8581, Japan*

(Received 14 September 2001; revised manuscript received 22 January 2002; published 10 May 2002)

The phonon dynamics of the spin-ladder vanadium oxides AV_2O_5 (A = Na,Ca,Mg,Cs) is studied using infrared and Raman spectroscopy techniques. The infrared-active phonon frequencies are obtained by Kramers-Kronig analysis of the reflectivity data. The assignment of the phonon modes in $(Ca,Mg,Cs)V_2O_5$ is based on the shell model lattice dynamical calculation of α'-NaV_2O_5. The large phonon frequency (448 cm^{-1}) renormalization in the sodium-deficient samples is found to be similar to the resonant-induced phonon renormalization in the nominally pure α'-NaV_2O_5. In the Raman spectra of CaV_2O_5 and MgV_2O_5 we observed the phonon overtones and combinational lines up to the fourth order. No spin-related modes are found in CsV_2O_5.

I. INTRODUCTION

Recently, the low-dimensional quantum spin systems, such as the spin-Peierls, spin-ladder, and the antiferromagnetic linear chain systems, have attracted much attention.[1] The vanadate family of AV_2O_5 oxides (A = Li,Na,Cs,Mg, Ca), which have common VO_5 square pyramids in the structure, have demonstrated a variety of the low-dimensional quantum spin phenomena such as one-dimensional antiferromagnetism in α'-NaV_2O_5 (Ref. 2) and LiV_2O_5 (Ref. 3), the antiferromagnetic two-leg ladder structure in CaV_2O_5 (Ref. 4) and MgV_2O_5 (Ref. 3), and the spin-dimer structure in CsV_2O_5 (Ref. 5).

The sodium vanadate (α'-NaV_2O_5) has an orthorhombic unit cell[6] with centrosymmetric space group $Pmmn$ and Z = 2. Such a crystalline structure assumes only one crystallographic position of vanadium atoms in the mixed-valence state (formal oxidation state is +4.5). Each vanadium atom is surrounded by five oxygen atoms, forming VO_5 pyramids. These pyramids are mutually connected via common edges to form layers in the (ab) plane. The Na (Ca,Mg) atoms are situated between these layers as intercalants. A schematic representation of one layer of AV_2O_5 (A = Na,Ca,Mg) crystal structure is given in Fig. 1(a). Please note that in the rest of the paper we label the crystallographic axes of Na, Ca, and Mg vanadates in a unified manner: in each case the (ab) plane contains the layer of AV_2O_5, with the b axis along the leg and the a axis along the rung of the ladder. The c axis is perpendicular to the layers. This notation is the same as in α'-NaV_2O_5 (Ref. 6) and CaV_2O_5 (Refs. 7 and 8) but different from some original papers dealing with crystal structure of MgV_2O_5 (Ref. 9). In this way, and to avoid confusion, we simplified discussion.

CaV_2O_5 is isostructural with α'-NaV_2O_5. The crystal structure of MgV_2O_5 is C-centered orthorhombic with nearly the same a and b axes as $Na(Ca)V_2O_5$ but with twice as large the c axis. The unit cell of this crystal consists of two layers, as is shown in Fig. 1(b). The crystal structure of monoclinic CsV_2O_5 is also a layered one,[10] with cesium ions situated

between the layers, Fig. 1(c). Each layer consists of VO_5 corner sharing square pyramids linked to VO_4 tetrahedra. The average V-O distance as a function of the coordination and oxidation number suggests that the V^{4+} and V^{5+} ions are segregated within the square pyramids and the tetrahedra, respectively.[10] The crystallographic parameters, given in Table I, will be discussed in details later.

The main difference between properties of $Ca(Mg)V_2O_5$ and α'-NaV_2O_5 is the fact that in the latter material the spins are not attached to a single V ion but to V-O-V molecular orbital of the rung.[11,12] In the case of $Ca(Mg)V_2O_5$ the S = 1/2 spins are attached to each V ion.

However, in spite of good understanding of the magnetic properties, the study of the vibrational properties of AV_2O_5 is of a great importance because of the still puzzling interplay between the charge and the magnetic ordering in α'-NaV_2O_5. Lattice dynamics for AV_2O_5 were studied only for α'-NaV_2O_5 in the framework of the shell[13,14] and the rigid ion model[15] calculations. A Raman scattering study of $Ca(Mg)V_2O_5$ is presented in Ref. 16. There, we focused mainly on the magnetic excitations. The vibrational properties of LiV_2O_5 single crystals were already reported in Ref. 17, and we do not include them in this paper. To the best of our knowledge there are no published data on the vibrational properties of CsV_2O_5.

In this work we present the infrared and Raman spectra of $(Ca,Mg,Cs)V_2O_5$ polycrystalline samples as well as of sodium-deficient $Na_xV_2O_5$ single crystals. The assignment of vibrational modes in $(Ca,Mg,Cs)V_2O_5$ oxides is done using the lattice dynamics of α'-NaV_2O_5.

II. EXPERIMENT

The present work was performed on single-crystal plates of $Na_xV_2O_5$ ($0.85 < x < 1.00$) with dimensions typically about $2 \times 4 \times 0.5$ mm^3 in the a, b, and c axes, respectively. In the case of $(Ca,Mg,Cs)V_2O_5$ we used powder samples. The details of the sample preparation were published elsewhere.[3,18] The infrared measurements were carried out with a BOMEM DA-8 FIR spectrometer. A DTGS pyroelec-
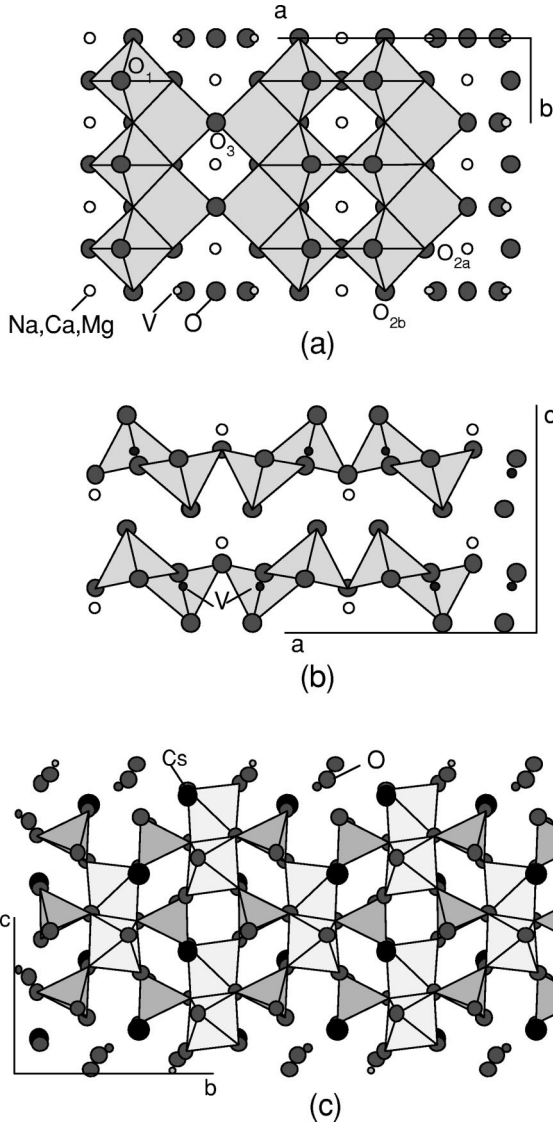
FIG. 1. Schematic representation of the AV_2O_5 crystal structure in the (a) (001) and (b) (010) planes. (c) Schematic representation of CsV_2O_5 crystal structure.

tric detector was used to cover the wave number region from 100 to 700 cm^{-1}; a liquid-nitrogen-cooled HgCdTe detector was used from 500 to 5000 cm^{-1}. Spectra were collected with 2 cm^{-1} resolution, with 1000 interferometer scans

TABLE I. Selected interatomic distances (in Å) and angles (in degrees) of AV_2O_5 ($A=$Na, Ca, Mg).

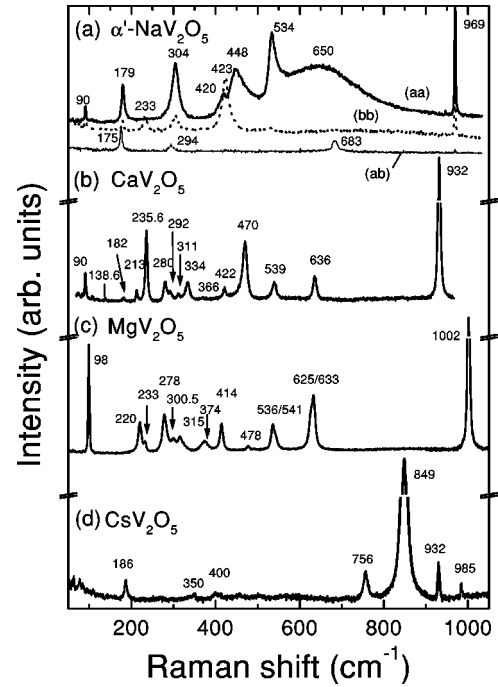|	α'-NaV$_2$O$_5$	CaV$_2$O$_5$	MgV$_2$O$_5$
V-O$_1$	1.61	1.645	1.618
V-O$_{2a}$	1.985	1.982	1.971
V-O$_{2b}$	1.9129	1.949	1.9575
V-O$_3$	1.8234	1.905	1.971
V^a-V^a	3.44	3.49	3.37
V^a-V^b	3.03	3.03	2.98
V-O$_3$-V	140.9	132.9	117.5

FIG. 2. (a) Room-temperature polarized Raman spectra of α'-NaV$_2$O$_5$. $\lambda_L=488$ nm. Unpolarized Raman spectra of CaV$_2$O$_5$ (b), MgV$_2$O$_5$ (c), and CsV$_2$O$_5$ (d). $\lambda_L=514.5$ nm.
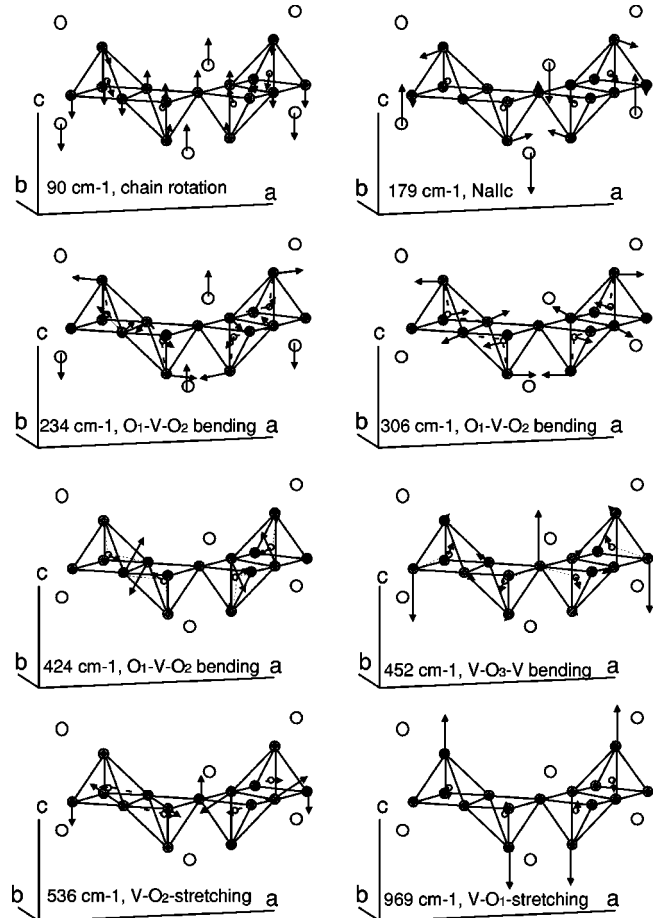

FIG. 3. Ion displacement patterns of Raman-active modes of A_{1g} symmetry in Na(Ca)V$_2$O$_5$.

TABLE II. Raman mode frequencies (in cm^{-1}) of AV$_2$O$_5$ (A= Na, Ca, Mg).

Symmetry	α'-NaV$_2$O$_5$ Obs.	(Ref. 14) Calc.	CaV$_2$O$_5$ Obs.	MgV$_2$O$_5$ Obs.	Assignment Ref. 14
A_g	90	102	90	98	chain rotation
	179	159	138.6	-	Na(Ca)$\parallel$c
	233	227	235.6	233	O-V-O bending
	304	298	?	?	O-V-O bending
	423	385	422	414	O-V-O bending
	448	466	470	478	V-O$_3$-V bending
	534	501	539	536	V-O$_2$ stretching
	969	949	932	1002	V-O$_1$ stretching
B_{1g}	175	182	182	-	chain rotation
	294	293	292	300.5	O-V-O bending
	683	685	636	625	V-O$_2$ stretching
B_{3g}	-	128	-	-	chain rotation
	-	232	-	-	Na$\parallel$b
	260	274	280	278	O-V-O bending
	366	373	366	374	V-O$_3$-V bending
	684	680	636	633	V-O$_2$ stretching
B_{2g}	149	143	-	-	Na$\parallel$a
	192	170	-	-	chain rotation
	226	223	213	220	O-V-O bending
	-	227	311	315	O-V-O bending
	-	383	334	323	O-V-O bending
	-	497	-	-	V-O$_2$ stretching
	550	535	-	541	V-O$_3$ stretching
	954	966	-	-	V-O$_1$ stretching

added for each spectrum. The Raman spectra were measured in the backscattering configuration using micro-Raman system with DILOR triple monochromator including a liquid-nitrogen-cooled charge-coupled device (CCD) detector. The Ar- and Kr-ion lasers were used as excitation sources.

III. RESULTS AND DISCUSSION

A. α'-Na$_x$V$_2$O$_5$

The room-temperature Raman spectra of α'-NaV$_2$O$_5$ from the (001) plane, for parallel and crossed polarizations, are given in Fig. 2(a). The spectra for parallel polarizations consist of A_g symmetry modes. Seven modes at 90, 179, 304, 420, 448, 534, and 969 cm^{-1} are clearly seen for the (aa) polarization and one additional mode at 233 cm^{-1} for the (bb) polarization. For the crossed (ab) polarization three Raman-active B_{1g} symmetry modes at 175, 294, and 683 cm^{-1} are observed. These spectra, previously published in Refs. 13, 14, 19, and 20, are fully in agreement with the same spectra published from other authors.[15,21–23] The assignment of all optical modes of α'-NaV$_2$O$_5$ is given in our previously published papers (Refs. 13 and 14) and we do not repeat it here in detail. Figure 3 represents the ionic displacement patterns of all A_g symmetry modes, obtained by shell model calculations.[14] According to Fig. 3, the phonon modes in the spectral range between 200 and 500 cm^{-1} originate from the bond bending vibrations, while the higher-frequency modes originate from the stretching vibrations of V-O atoms. The shorter V-O distance gives the higher mode frequency. Thus, the highest-frequency mode at 969 cm^{-1}, Fig. 2(a), represents V-O$_1$ stretching vibrations, while the modes at about 600 cm^{-1} originate from V-O$_2$ stretching vibrations, Table II. Note that the Raman mode at 448 cm^{-1}, which originates from V-O$_3$-V bending vibrations (mostly vibration of O$_3$ atoms along the c axis), should be sensitive to Na deficiency since the Na vacancy produces the change of bending angle and/or it can modify the bond-bending force constant due to redistribution of the electron density.

Since the electrons in α'-NaV$_2$O$_5$ are located in a V-O$_3$-V molecular orbital, we paid the special attention to the 448 cm^{-1} mode in the sodium-deficient samples. Figure 4 shows the Raman spectra of Na$_x$V$_2$O$_5$ samples for x between 1.00 and 0.96. As can be seen from Fig. 4, a weak additional mode at about 485 cm^{-1} seems to appear due to a Na deficiency. This effect is also observed in Refs. 15 and 23. In order to extract the frequencies and intensities of the Raman modes we deconvoluted the Raman spectra in the spectral range from 350 to 950 cm^{-1} into two Lorentzians (mode at 420 and 485 cm^{-1}), two Fano-profile mode (asymmetric modes at 448 and 531 cm^{-1}), and the Gausian-profile mode (650 cm^{-1}). From the fitting procedure we concluded that the intensity of the 448 cm^{-1} mode decreases by in-

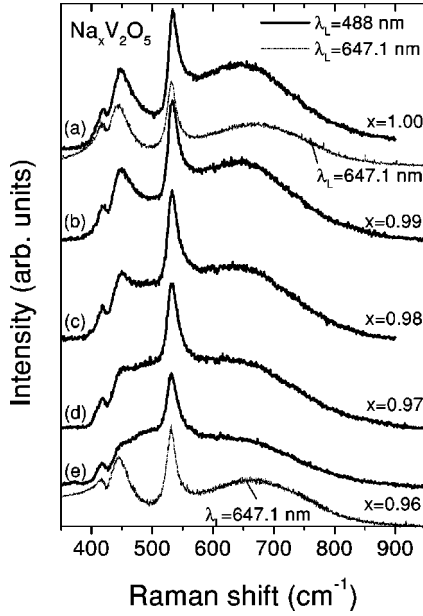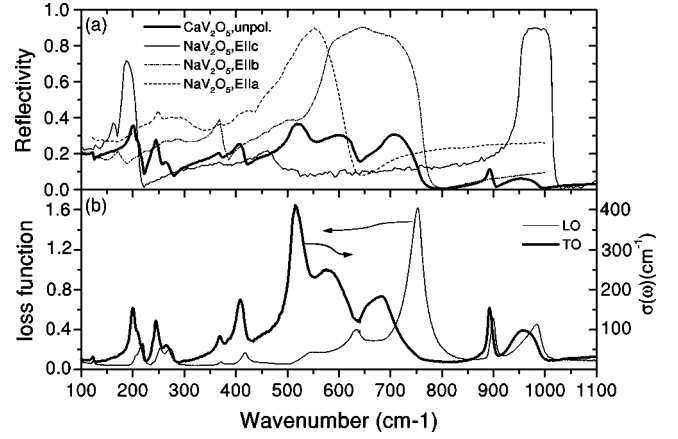FIG. 4. Room-temperature (aa) polarized Raman spectra of α'-Na$_x$V$_2$O$_5$ in the spectral range 350–950 cm^{-1}.

FIG. 5. (a) Room-temperature unpolarized far-infrared reflectivity spectra of CaV$_2$O$_5$ together with the polarized far-infrared spectra of α'-NaV$_2$O$_5$. (b) $\sigma(\omega)$ and $-\mathrm{Im}[1/\epsilon(\omega)]$ vs frequency dependences obtained by Kramers-Kronig analysis of CaV$_2$O$_5$ reflectivity data.

creasing the Na deficiency, without a change of its intrinsic frequency; the 531 cm^{-1} mode changes its asymmetry because of a slight shift of the broad structure at 650 cm^{-1} and due to appearance of the new mode at 485 cm^{-1}; this new mode exhibits continous intensity increase as a function of sodium deficiency.

As discussed by Bacsa *et al.*[23] the 448 cm^{-1} phonon renormalization in sodium-deficient samples is caused by increase of the number of V^{5+}-O$_3$-V^{5+} bonds. This conclu-

sion is based on the fact that corresponding mode in V$_2$O$_5$ is at 483 cm^{-1} (Ref. 24) (in V$_2$O$_5$ only vibrations of the V^{5+}-O$_3$-V^{5+} bonds are present). However, the Raman spectra of Na$_x$V$_2$O$_5$ (especially the energy region between 400 and 700 cm^{-1}) depend strongly on the laser line used.[20] It is interesting to note that 448 cm^{-1} mode renormalization is not observed in the Raman spectra of Na$_{0.96}$V$_2$O$_5$ measured with 647.1 nm laser line, Fig. 4(e). Thus, the phonon renormalization could be just resonant effect, associated with a p-d electronic transition at about 3.2 eV.[25,26] In this case, the renormalization is caused by increase of the number of V^{4+}-O$_3$-V^{4+} bonds due to optical transitions of electrons

TABLE III. Infrared-active mode frequencies (in cm^{-1}) of AV$_2$O$_5$ (A = Na, Ca, Mg).

Symmetry	α'-NaV$_2$O$_5$ Obs.	(Ref. 14) Calc.	CaV$_2$O$_5$ Obs.	MgV$_2$O$_5$ Obs.	Assignment Ref. 14
B_{1u}	164/166	160/160	198/218	213/215	chain rotation
	181/212	174/175	-	-	A‖c
	-	277/277	264/272	-	O-V-O bending
	(368/370)	375/375	-	-	O-V-O bending
	460/480	478/478	-	-	V-O$_3$-V bending
	-	488/488	-	-	V-O$_2$ stretching
	955/1014	945/945	956.5/983	1024/1038.5	V-O$_1$ stretching
B_{2u}	178/183	167/177	122.6/123	115/116.5	O-V-O bending+A‖b
	230.5/231	232/260	-	-	A‖b
	370/378	374/376	368.6/371	-	V-O$_3$-V bending
	582/762	568/764	578.6/753	577/696	V-O$_2$ stretching
B_{3u}	138/138.2	135/137	-	-	chain transl. ‖c
	144.5/144.7	158/158	-	-	A‖a
	254/256	252/264	244/253	284/297	O-V-O bending
	438/439	405/405	408/417.4	416/422	O-V-O bending
	469/473	486/486	-	-	V-O$_2$ stretching
	505/624	534/536	515/633	510/629.5	V-O$_3$ stretching
	939.8/940	953/960	892/900	958/964	V-O$_1$ stretching

from O_p to d_{xy} states.[26] So the bond bending phonon energy (under resonance) should be compared with the corresponding mode in CaV$_2$O$_5$ (470 cm^{-1}). A more detailed study of the resonance effects in Na-deficient samples is a subject of our forthcoming paper.[27]

The sodium deficiency also influences the 650 cm^{-1} structure (the frequency shift of 20 cm^{-1} is recorded by a decrease of x from 1 to 0.96). The nature of this broad structure, observed in α'-NaV$_2$O$_5$ only for (aa) polarization, is not yet understood.[15,21–23]

B. CaV$_2$O$_5$

The factor-group analysis for CaV$_2$O$_5$ crystal predicts

$$\Gamma_{(Na,Ca)V_2O_5} = 8A_g(aa,bb,cc) + 3B_{1g}(ab) + 8B_{2g}(ac)$$
$$+ 5B_{3g}(bc) + 7B_{1u}(\mathbf{E}\|c) + 4B_{2u}(\mathbf{E}\|b)$$
$$+ 7B_{3u}(\mathbf{E}\|a).$$

According to this representation one can expect 24 Raman- and 18 infrared-active modes. The room-temperature unpolarized reflectivity spectra of CaV$_2$O$_5$ in the spectral range from 100 to 1100 cm^{-1} is given in Fig. 5(a). In Fig. 5(b) we shown the $\sigma(\omega)$ and the $-\text{Im}[1/\epsilon(\omega)]$ spectra. These spectra are obtained using Kramers-Kronig analysis of reflectivity data from Fig. 5(a). The TO and LO mode frequencies, given in Table III, were obtained as peak positions of $\sigma(\omega)$ and $-\text{Im}[1/\epsilon(\omega)]$, respectively. According to Fig. 5 and Table III, we observed ten oscillators. The assignment given in Table III is done by comparison of un-polarized CaV$_2$O$_5$ spectrum with polarized infrared reflectivity spectra of isostructural α'-NaV$_2$O$_5$. The polarized far-infrared reflectivity spectra of α'-NaV$_2$O$_5$ were published by us in Ref. 14. These spectra, Fig. 5(a), are completely in agreement with results of other groups[28–31] for $\mathbf{E}\|b$ and $\mathbf{E}\|c$ polarizations. In the case of $\mathbf{E}\|a$ polarization we found that better agreement between experimental and calculated reflectivity occurs when two oscillators with TO frequencies at about 438 cm^{-1} and 469 cm^{-1} are added. In fact, these two oscillators are not clearly pronounced even at low temperatures.[29,31] Because of that, their existence is questionable.

The reflectivity measurements carried out on polycrystalline samples give good results for TO and LO mode frequencies in the case of isolated oscillators only. Two highest-frequency oscillators of CaV$_2$O$_5$ were assigned as V-O$_1$ stretching modes polarized along the a (892 cm^{-1}) and c axes (956 cm^{-1} mode). In α'-NaV$_2$O$_5$ reflectivity spectra in the spectral range between 500 and 800 cm^{-1}, there are two oscillators of different symmetry. Note that these oscillators appear as three-peak structure in the same spectral region in the reflectivity spectra of polycrystalline CaV$_2$O$_5$. The three peak structure is also found in the case of α'-NaV$_2$O$_5$ when polarization was changed between a and b axes (see Fig. 11 in Ref. 31). The assignment of the infrared-active modes for frequencies lower than 500 cm^{-1} is very difficult without single crystal samples. Consequently, the assignment given for these oscillators in Table III is tentative.

The unpolarized Raman spectrum of CaV$_2$O$_5$ is presented in Fig. 2(b). The assignment of the observed Raman modes is given in Table II by comparison between mode intensities for parallel and crossed polarized configurations[16] with fully polarized spectra of α'-NaV$_2$O$_5$. Despite the same crystal structure of CaV$_2$O$_5$ and α'-NaV$_2$O$_5$ there is significant frequency difference for some of analogous phonon modes, due to the difference in masses of metal ions, interatomic distances, and the electronic structure. The highest-frequency phonon mode appears in CaV$_2$O$_5$ Raman spectra at 932 cm^{-1} (37 cm^{-1} lower then in α'-NaV$_2$O$_5$). This mode of the A_{1g} symmetry represents the V-O$_1$ bond stretching vibration (Table II, Fig. 3). The larger V-O$_1$ distance in CaV$_2$O$_5$, in comparison with the same interatomic distance in α'-NaV$_2$O$_5$ (see Table I), causes the frequency shift of this phonon to lower energies. The same conclusion can be drawn for the CaV$_2$O$_5$ mode of the B_{1g} symmetry at 636 cm^{-1}. The mode originates from bond stretching vibrations of V and O$_{2b}$ ions along the b axis. Its frequency is 48 cm^{-1} lower than the corresponding B_{1g} mode of α'-NaV$_2$O$_5$ since the V-O$_{2b}$ distance in CaV$_2$O$_5$ is considerably larger then the same distance in α'-NaV$_2$O$_5$ (see Table I). The next A_{1g} mode of CaV$_2$O$_5$ appears at frequency 539 cm^{-1} which is close to the frequency of analogous mode in α'-NaV$_2$O$_5$ (534 cm^{-1}). This mode represents the bond stretching vibration of V and O$_{2a}$ ions (see Fig. 3). No significant frequency difference between these modes is in accordance with a similar value of the V-O$_{2a}$ bond length in CaV$_2$O$_5$ and α'-NaV$_2$O$_5$; see Table I. The A_{1g} mode at 470 cm^{-1} shows a remarkable frequency shift to higher frequency in comparison with the corresponding mode of α'-NaV$_2$O$_5$ (448 cm^{-1}). This mode represents the bond bending vibrations of V-O$_3$-V bond (mainly O$_3$ ion vibrations along the c axis, Fig. 3). According to the crystallographyic data this mode should appear at frequency lower than the frequency of analogous mode in α'-NaV$_2$O$_5$, because the V-O$_3$-V bond length in CaV$_2$O$_5$ (see Table I) is larger than that of the α'-NaV$_2$O$_5$. In fact, this is expected, if we have in mind that the renormalized frequency of V-O$_3$-V bond bending mode in α'-NaV$_2$O$_5$ (485 cm^{-1}) when two electrons are induced in the V-O$_3$-V orbital (Sec. III A).

The assignment of the bond bending modes of CaV$_2$O$_5$ in the 180–350 cm^{-1} spectral region, given in Table II, should be considered as tentative one. Only single-crystal measurements can resolve different symmetry modes of crossed polarizations in this spectral region. The lowest-frequency mode, which represents the chain rotation, appears at 90 cm^{-1} in both Na and Ca vanadates. The mode at 136 cm^{-1} we tentatively assign as Ca atom vibration since its frequency is close to calculated value if we consider mass effect only. Namely, the replacement of lighter Na atoms with heavier Ca produces the shift of the corresponding mode towards lower frequencies according to $(\omega_{Na} = 179 \text{ cm}^{-1}) \times (m_{Na}/m_{Ca})^{1/2} = 135.7 \text{ cm}^{-1}$, which is very close to the observed value.

Figures 6(a) and 6(b) show Raman spectra of α'-NaV$_2$O$_5$ and CaV$_2$O$_5$ measured at room temperature in the spectral range from 400 to 2300 cm^{-1}. All modes with energies

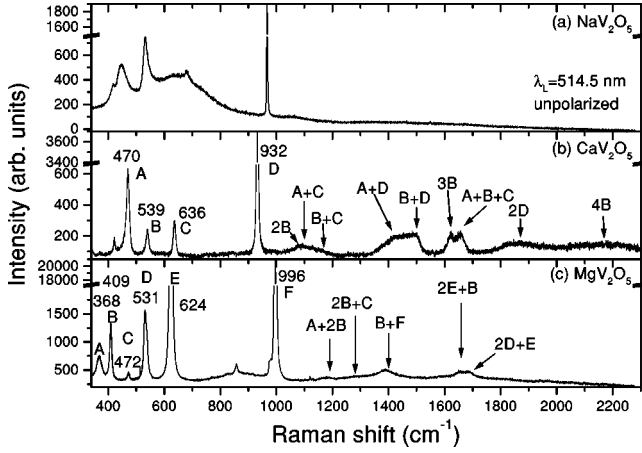FIG. 6. Room-temperature Raman scattering spectra of α'-NaV$_2$O$_5$ (a), CaV$_2$O$_5$ (b) and MgV$_2$O$_5$ (c) in the spectral range $400-2300$ cm^{-1}. $\lambda_L = 514.5$ nm.
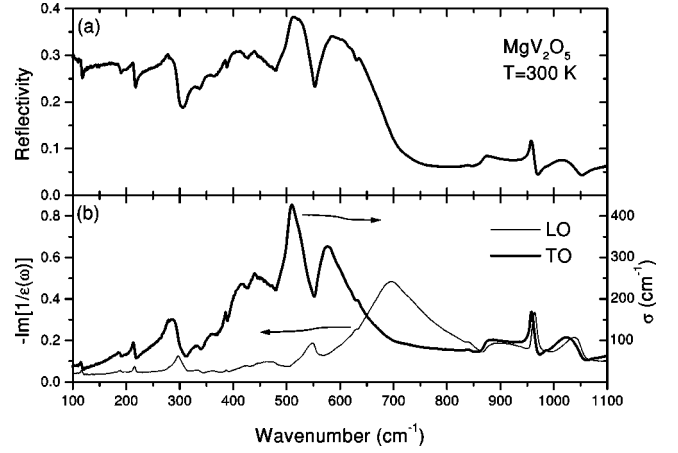

FIG. 7. (a) Room-temperature far-infrared reflectivity spectra of MgV$_2$O$_5$. (b) $\sigma(\omega)$ and $-\mathrm{Im}[1/\epsilon(\omega)]$ vs frequency dependences obtained by Kramers-Kronig analysis of MgV$_2$O$_5$ reflectivity data.

higher than 1000 cm^{-1} have two-phonon character. In the case of CaV$_2$O$_5$ we observed not only overtones ($2B$, $2D$, $3B$, $4B$) but also combinational lines. At this stage is not clear why the combinational lines have stronger intensity than overtones. We believe that this effect results from resonant conditions. However, there is no experimental data about the electronic structure (energy gap) in this material, so it is not possible to discuss this effect in more detail.

C. MgV$_2$O$_5$

MgV$_2$O$_5$ has a C-centered orthorhombic unit cell[9] with parameters $a = 0.3696$ nm, $b = 0.9965$ nm, and $c = 1.1019$ nm and space group $Cmcm$ (D_{2h}^{17}). In our setting, shown in Fig. 1(b) (cab setting), the space group is $Amma$. The MgV$_2$O$_5$ unit cell consists of four formula units ($Z = 4$) comprising 32 atoms in all. The site symmetries of V, Mg, O$_1$, O$_2$, and O$_3$ atoms in (D_{2h}^{17}) space group are ($8f$), ($4c$), ($8f$), ($8f$), and ($4c$) respectively. Factor-group analysis (FGA) yields

$$(\mathrm{Mg},\mathrm{O}_3)(C_{2v}^z):\Gamma = A_g + B_{3g} + B_{1u} + B_{2g} + B_{2u} + B_{3u},$$

$$(\mathrm{V},\mathrm{O}_1,\mathrm{O}_2)(C_s^{xz}):\Gamma = 2A_g + A_u + B_{1g} + 2B_{1u} + 2B_{2g} + B_{2u}$$

$$+ B_{3g} + 2B_{3u}.$$

Summarizing these representations and subtracting the acoustic ($B_{1u} + B_{2u} + B_{3u}$) and silent (A_u) modes, we obtained the following irreducible representations of MgV$_2$O$_5$ vibrational modes of $Amma$ space group:

$$\Gamma_{\mathrm{MgV_2O_5}}^{opt.} = 8A_g(aa,bb,cc) + 3B_{1g}(ab) + 8B_{2g}(ac)$$

$$+ 5B_{3g}(bc) + 7B_{1u}(\mathbf{E}\|c) + 4B_{2u}(\mathbf{E}\|b)$$

$$+ 7B_{3u}(\mathbf{E}\|a).$$

Thus, 18 infrared- and 24 Raman-active modes are expected in the MgV$_2$O$_5$ spectra.

The room-temperature unpolarized far-infrared reflectivity spectrum of MgV$_2$O$_5$ in the spectral range from 100 to 1100 cm^{-1} is given in Fig. 7(a). Figure 7(b) shows the $\sigma(\omega)$ and the $-\mathrm{Im}[1/\epsilon(\omega)]$ spectra, obtained using Kramers-Kronig analysis of reflectivity data from Fig. 7(a). As it is illustrated in Table III, it was not difficult to assign the oscillators with TO/LO frequencies above 500 cm^{-1} by comparison with corresponding spectra of α'-NaV$_2$O$_5$ and CaV$_2$O$_5$. Below 500 cm^{-1} the assignment was practically impossible due to many oscillators of different symmetry. Assignment of the Raman spectra of MgV$_2$O$_5$ [see Fig. 2(c)] is done in the same way as in the CaV$_2$O$_5$ case. The results are collected in Table II. The Raman spectrum of MgV$_2$O$_5$ in the wide spectral range up to 2300 cm^{-1} is given in Fig. 6(c). As in the case of CaV$_2$O$_5$ we observed first- and second-order Raman modes as well as combinational modes of overtones.

D. CsV$_2$O$_5$

The unit cell of CsV$_2$O$_5$ consists of four formula units ($Z = 4$) with 32 atoms in all. Since there is a large number of atoms in the unit cell, we can expect a large number of optically active modes. All atoms have $4(e)$ position symmetry of $P2_1/c$ (C_{2h}^5) space group.[10] Factor-group analysis yields the following distribution of vibrational modes:

$$\Gamma_{\mathrm{CsV_2O_5}} = 24A_g(aa,bb,cc,ab) + 24B_g(ac,bc)$$

$$+ 24A_u(\mathbf{E}\|c) + 24B_u(\mathbf{E}\|a,\mathbf{E}\|b).$$

According to this representation one can expect 48 infrared- and 48 Raman-active modes. Experimentally, the number of observed modes is less than 25 for each spectroscopic method; see Table IV.

Far-infrared spectra of CsV$_2$O$_5$ together with results of Kramers-Kronig analysis are given in Figs. 8(a) and 8(b), respectively. If we compare this reflectivity spectra with the infrared reflectivity spectra of other vanadates, we can conclude that the two highest-frequency modes, as well as the modes between 500 and 700 cm^{-1}, represent the vibration of VO$_5$ pyramid. The modes between 750 and 950 cm^{-1} are

TABLE IV. Mode frequencies (in cm^{-1}) of CsV$_2$O$_5$.

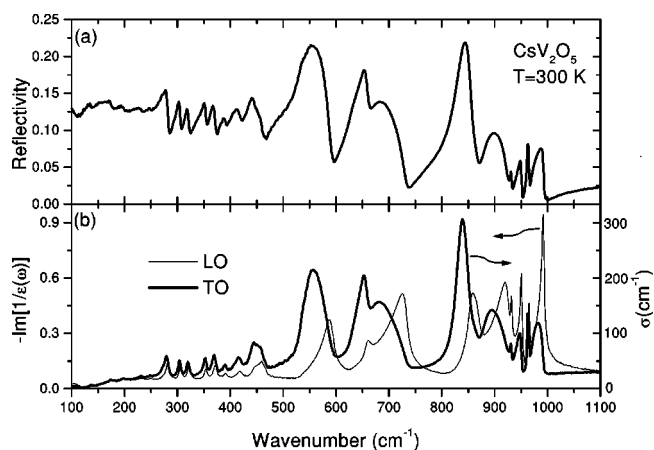| Raman		Infrared (300 K)	
300 K	10 K	TO	LO
108	109	136	136
-	151	174	175
-	166	198	199
186	186.5	231	232
-	199.5	248	248.5
-	225.5	279	282
-	235	304	305
-	251	320	321
298	299	352	354
-	337	369	371
350	350	390	391
400	398	415	418
411	413	445	446.5
-	434	450	452.5
456	462	457	459.4
501	509	556	587
712	715	653	660.5
756	762	681	725
784	790	839	858
849	846	895	920
932	932	930.5	931
985	986	947	951
		962	965
		981.6	992

FIG. 8. (a) Far-infrared reflectivity spectra of CsV$_2$O$_5$. (b) $\sigma(\omega)$ and $-\text{Im}[1/\epsilon(\omega)]$ vs frequency dependences obtained by Kramers-Kronig analysis of reflectivity data.

500 cm^{-1} are the bond bending modes of the same structural units. The highest-frequency mode at 985 cm^{-1} represents V-O^{apical} vibration of VO$_5$ pyramid, because this is the shortest bond in CsV$_2$O$_5$.[10] The modes at 784, 849, and 932 cm^{-1} originate from V-O stretching vibration of the corresponding bonds of VO$_4$ tetrahedra. The frequencies of observed infrared and Raman modes of CsV$_2$O$_5$ are collected in Table IV.

In conclusion, we have studied the phonon dynamics of spin ladder vanadate oxides AV$_2$O$_5$ (A = Na, Ca, Mg, Cs) using infrared and Raman spectroscopy techniques. The assignment of the phonon modes in (Ca,Mg,Cs)V$_2$O$_5$ is done on the basis of the shell model lattice dynamical calculations for α'-NaV$_2$O$_5$. The Raman spectra of the Na-deficient samples have a renormalization of the 448 cm^{-1} phonon frequency in a way similar to that in a nominally pure α'-NaV$_2$O$_5$ sample under resonant conditions. We observed the overtones and combinational lines up to fourth order in the Raman spectra of CaV$_2$O$_5$ and MgV$_2$O$_5$. No spin-related modes are found in CsV$_2$O$_5$.

bond stretching vibrations of VO$_4$ tetrahedra. In the spectral range below 500 cm^{-1} there are many modes that originate from V-O bond bending vibration. As in the case of Raman spectra the more precise assignment of infrared active modes is not possible without single crystal measurements.

Figure 2(d) shows unpolarized room-temperature Raman spectra of CsV$_2$O$_5$ in the 100–1000 cm^{-1} spectral region, excited with 514.5 nm energy. We observed 14 modes at room temperature and 8 additional modes at T = 10 K. No spin-related modes are observed in CsV$_2$O$_5$. The unobserved modes are probable of very low intensity and we could not resolve them from the level of noise. As can be seen from Fig. 2(d), the Raman modes of CsV$_2$O$_5$ are grouped into two spectral region. Above 700 cm^{-1} are the bond stretching mode of VO$_4$ tetrahedra and VO$_5$ pyramids and below

*Permanent address: Institute of Physics-Belgrade, P. O. Box 68, 11080 Belgrade/Zemun, Yugoslavia.

[1] E. Dagotto and T.M. Rice, Science **271**, 618 (1996).

[2] M. Isobe and Y. Ueda, J. Phys. Soc. Jpn. **65**, 1178 (1996).

[3] M. Isobe, Y. Ueda, K. Takizawa, and T. Goto, J. Phys. Soc. Jpn. **67**, 755 (1998).

[4] H. Iwase, M. Isobe, Y. Ueda, and H. Yasuoka, J. Phys. Soc. Jpn. **65**, 2397 (1996).

[5] M. Isobe and Y. Ueda, J. Phys. Soc. Jpn. **65**, 3142 (1996).

[6] H.G. von Schnering, Yu. Grin, M. Kaupp, M. Somer, R.K. Kre-mer, O. Jepsen, T. Chatterji, and M. Weiden, Z. Kristallogr. **213**, 246 (1998).

[7] M. Onoda and N. Nishiguchi, J. Solid State Chem. **127**, 359 (1996).

[8] M. Onoda and N. Nishiguchi, J. Phys.: Condens. Matter **11**, 3475 (1999).

[9] M. Onoda and N. Nishiguchi, J. Phys.: Condens. Matter **10**, 1229 (1998).

[10] K. Waltersson and B. Forslund, Acta Crystallogr., Sect. B: Struct. Crystallogr. Cryst. Chem. **33**, 789 (1977).

[11] P. Horsch and F. Mack, Eur. Phys. J. B **5**, 367 (1998).

[12] N. Suaud and M.B. Lepetit, Phys. Rev. B **62**, 402 (2000).

[13] Z.V. Popović, M.J. Konstantinović, R. Gajić, V. Popov, Y.S. Raptis, A.N. Vasil'ev, M. Isobe, and Y. Ueda, J. Phys.: Condens. Matter **10**, L513 (1998).

[14] Z.V. Popović, M.J. Konstantinović, R. Gajić, V. Popov, Y.S. Raptis, A.N. Vasil'ev, M. Isobe, and Y. Ueda, Solid State Commun. **110**, 381 (1999).

[15] M.N. Popova, A.B. Sushkov, S.A. Golubchik, B.N. Mavrin, V.N. Denisov, B.Z. Malkin, A.I. Iskhakova, M. Isobe, and Y. Ueda, Zh. Éksp. Teor. Fiz. **115**, 2170 (1999) [JETP **88**, 1186 (1999)].

[16] M.J. Konstantinović, Z.V. Popović, M. Isobe, and Y. Ueda, Phys. Rev. B **61**, 15 185 (2000).

[17] Z.V. Popović, R. Gajić, M.J. Konstantinović, R. Provoost, V.V. Moshchalkov, A.N. Vasil'ev, M. Isobe, and Y. Ueda, Phys. Rev. B **61**, 11 454 (2000).

[18] M. Isobe, C. Kagami, and Y. Ueda, J. Cryst. Growth **181**, 314 (1997).

[19] M.J. Konstantinović, Z.V. Popović, A.N. Vasil'ev, M. Isobe, and Y. Ueda, Solid State Commun. **112**, 397 (1999).

[20] M.J. Konstantinović, Z.V. Popović, T. Ruf, M. Cardona, A.N. Vasil'ev, M. Isobe, and Y. Ueda, Phys. Status Solidi B **215**, 661 (1999).

[21] H. Kuroe, H. Sato, T. Sekine, M. Isobe, and Y. Ueda, J. Phys. Soc. Jpn. **67**, 2881 (1998).

[22] M. Fischer, P. Lemmens, G. Els, G. Güntherodt, E.Ya. Sherman, E. Morre, C. Geibel, and F. Steglich, Phys. Rev. B **60**, 7284 (1999).

[23] W.S. Bacsa, R. Lewandowska, A. Zwick, and P. Millet, Phys. Rev. B **61**, R14 885 (2000).

[24] P. Clauws, J. Broeckx, and J. Vennik, Phys. Status Solidi B **131**, 459 (1985).

[25] M.J. Konstantinović, L.F. Lastras-Martinez, M. Cardona, Z.V. Popović, A.N. Vasil'ev, M. Isobe, and Y. Ueda, Phys. Status Solidi B **211**, R3 (1999).

[26] C. Presura, D. van der Marel, A. Damascelli, and R.K. Kremer, Phys. Rev. B **61**, 15 762 (2000).

[27] M. J. Konstantinović, Z. V. Popović, V. V. Moshchalkov, C. Presura, R. Gajić, M. Isobe, and Y. Ueda, cond-mat/0203298, Phys. Rev. B (to be published).

[28] D. Smirnov, P. Millet, J. Leotin, D. Poilblanc, J. Riera, D. Augier, and P. Hansen, Phys. Rev. B **57**, R11 035 (1998).

[29] A. Damascelli, D. van der Marel, M. Grüninger, C. Presura, T.T.M. Palstra, J. Jegoudez, and A. Revcolevschi, Phys. Rev. Lett. **81**, 918 (1998).

[30] D. Smirnov, J. Leotin, P. Millet, J. Jegoudez, and A. Revcolevschi, Physica B **259-261**, 992 (1999).

[31] A. Damascelli, C. Presura, D. van der Marel, J. Jegoudez, and A. Revcolevschi, Phys. Rev. B **61**, 2535 (2000).